Available online at www.sciencedirect.com

ScienceDirect

Energy Procedia 8 (2011) 275–281

Energy Procedia

SiliconPV: 17-20 April 2011, Freiburg, Germany

Modelling carrier recombination in highly phosphorus-doped industrial emitters

A. Kimmerle*, A. Wolf, U. Belledin, D. Biro

Fraunhofer Institute for Solar Energy Systems ISE, Heidenhofstr. 2, 79110 Freiburg, Germany

Abstract

One important parameter for modelling emitter recombination is the surface recombination velocity (SRV), which strongly depends on the surface doping concentration and the applied surface passivation. However, for highly phosphorus-doped surfaces with concentrations in excess of $2{\cdot}10^{20}$ cm^{-3}, where not all of the dopant is electrically activated, data is hardly available in the literature. Moreover, the bulk carrier lifetime in such supersaturated near surface regions is unknown. We use an analytical model to describe silicon-nitride-passivated phosphorus-diffused emitters. The model shows excellent agreement with a recently presented numerical solver, deviating less than 1 %. In both cases we apply a Fermi-Dirac statistics correction and account for band gap narrowing to calculate the intrinsic carrier density. Our results from measurements of the emitter dark saturation current density indicate that either the SRV or the local carrier lifetime in the supersaturated region are strongly affected by the doping concentration, even if it exceeds the dopant activation limit by far. Assuming only Auger recombination in the supersaturated region, we derive an upper limit for the SRV that depends on the chemical phosphorus surface concentration.

Selection and/or peer-review under responsibility of SiliconPV 2011

Keywords: Modelling, lifetime, passivation, emitter, recombination, dead-layer

1. Analytical modelling of emitter recombination

The modelling of highly doped regions is a complicated task, since the solution of the coupled transport and continuity equations strongly depends on material parameters which vary over several orders of magnitude in the devices of interest. There exist several programs like the new freeware

* Corresponding author. Tel.: +49-761-4588-5653; fax: +49-761-4588-9250.
E-mail address: achim.kimmerle@ise.fraunhofer.de

1876–6102 © 2011 Published by Elsevier Ltd. Selection and/or peer-review under responsibility of SiliconPV 2011.
Open access under CC BY-NC-ND license. doi:10.1016/j.egypro.2011.06.136

simulation tool EDNA [1], which solve this problem numerically. To obtain more flexibility and speed, we use the analytical 3rd order approximation from Cuevas et al. [2] to model the emitter under non-illuminated conditions. To compare the results of our analytical model with the numerical approach, we calculate the emitter dark saturation current density J_{0e} for two different doping profiles, applying the same physical models for minority carrier mobility [3, 4], Auger and radiative recombination [5], constant high Shockley-Read-Hall (SRH) carrier lifetime of τ_{SRH} = 1 ms in the bulk of the emitter and equilibrium minority hole concentration. For the latter the use of Fermi-Dirac (FD) statistics is required due to the high doping concentrations. Moreover, band gap narrowing (BGN) has to be considered. We apply FD statistics and the full random-phase approximation BGN model of Schenk [6] and take care to be consistent with the accepted intrinsic carrier density of $n_i = 9.65 \cdot 10^9$ cm^{-3} at T = 300 K [7] for undoped silicon (Appendix A). The results (Table 1) show very good agreement for both, the analytical approximation and the numerical solver EDNA [1], where the advantage of the analytical solution lies in its flexibility and speed.

Table 1. Analytically (this work, based on the approximation from Cuevas [2]) and numerically (EDNA [1]) evaluated dark saturation current densities J_{0e} at T = 300 K for a Gaussian profile and an electron concentration profile obtained from SIMS data (Fig 1). The p-type base doping is $N_A = 1.5 \cdot 10^{16}$ cm^{-3}.

Input Parameters					**Results for J_{0e} (fA/cm^2)**	
Profile	Electron surface concentration (cm^{-3})	Sheet resistance (Ω/sq.)	Junction depth (µm)	Assumed SRV (cm/s)	Analytical (this work)	Numerical (EDNA) from dark IV
Gaussian	$1 \cdot 10^{20}$	17	1.5	$1 \cdot 10^5$	134.7	134.1
Measured	$2.38 \cdot 10^{20}$	110	0.29	$7 \cdot 10^5$	119.6	118.4

2. Recombination at highly phosphorus-doped surface regions

The SRV of passivated emitters strongly depends on the surface concentration and surface passivation technology [8]. Industrial emitters exhibit high surface concentrations and high amounts of electrically inactive and undissolved dopant; however adequate data for the SRV at high surface concentrations and for bulk recombination in the supersaturated region (Fig 1) is hardly available. In this work, we first extract an upper limit for the SRV from measurements of J_{0e} using our analytical model by assuming only Auger and radiative recombination in the emitter bulk. We then compare our results to some assumptions for the bulk recombination in the supersaturated region.

2.1. Experiment

The starting material consists of boron-doped shiny etched float zone wafers with a specific resistivity of 1 Ωcm (see Fig 2). A tube furnace $POCl_3$-diffusion at 800 °C forms the emitter with an initial sheet resistance of R_{sheet} = 110 Ω/sq. After removal of the phosphosilicate glass, well controlled wet chemical etching removes between 0 and 36 nm of silicon from the surface yielding samples with surface concentrations between $1.3 \cdot 10^{21}$ and $4.8 \cdot 10^{19}$ cm^{-3}. On selected samples the doping profile is acquired by SIMS measurements. The thickness of the removed surface layer is evaluated from the comparison of doping profiles and sheet resistance measurements. Subsequently a SiN_x anti reflection layer is deposited on both sides by plasma enhanced chemical vapour deposition and the samples are exposed to a contact firing step in a conveyor belt furnace to facilitate hydrogen passivation. Then J_{0e} is extracted from QSSPC lifetime measurements in low-level injection [9] applying the same material parameters as in Section 1.

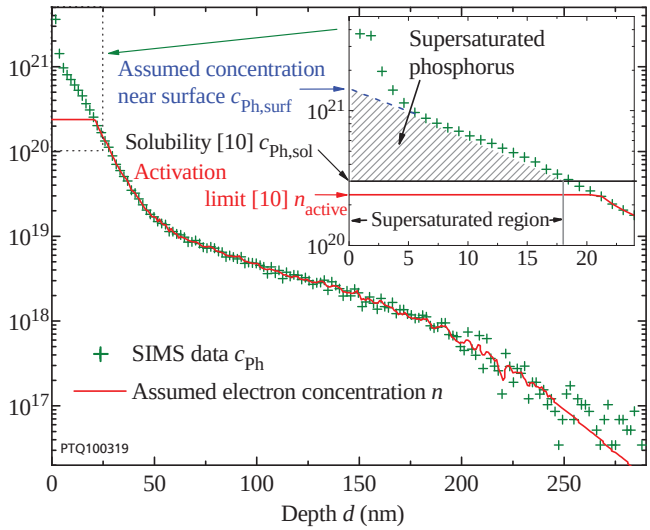

Fig 1. Chemical phosphorus concentration c_{Ph} profile from SIMS and calculated electron concentration n. The assumed activation limit of $n_{active} = 2.38 \cdot 10^{20}$ cm^{-3} agrees well with R_{sheet} measurements. In excess of the solubility limit $c_{Ph,sol} = 3 \cdot 10^{20}$ cm^{-3}, phosphorus is precipitated [10]

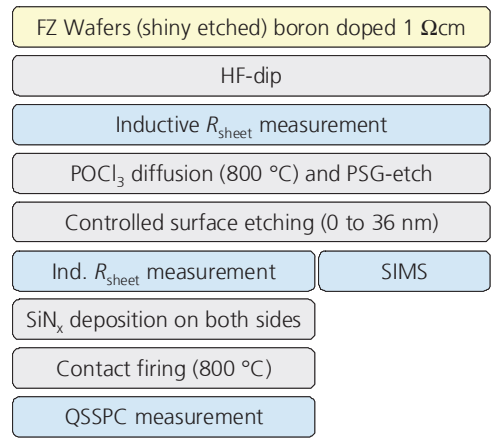

Fig 2. Process flow for the fabrication of symmetric emitter samples including characterisation steps

With the attained thickness of the removed silicon layer, the surface doping concentration is extracted from the emitter doping profile. Near the surface of all samples a measurement artefact occurs for which we correct by exponential extrapolating the first 5 nm of the doping profile of the not etched back emitter (see Fig 1). We then calculate the electron concentration profile from the doping profile (see Fig 1), assuming full dopant ionisation below the activation limit n_{active} [10], neglecting shifts between the carrier and the dopant profiles. For the activation limit we apply a temperature of 800 °C, since both, the emitter formation and the fast firing step take place at this temperature. The attained value of $n_{active} = 2.38 \cdot 10^{20}$ cm^{-3} agrees well with our sheet resistance measurements applying the carrier mobility model from Ref. [3, 4].

2.2. Analysis of SRV and bulk recombination

Recombination in industrial emitters is often strongly affected by the forming of P-Si precipitate structures close to the surface [11]. We therefore analyse our samples using both transmission and scanning electron microscopy. Typical precipitate structures are found on reference samples; however, the samples analysed here do not show evidence for precipitate formation near the surface. Thus it seems adequate to assume Auger recombination as the dominant recombination channel for samples where the supersaturated region has been removed. We consider four cases to model the SRV and the carrier recombination in the supersaturated region:

- Case 1: The minority carrier lifetime in the supersaturated region τ_{sat} is limited by Auger recombination. This leads to a constant lifetime of $\tau_{sat} = \tau_{Aug} = 133$ ps in the first 20 nm near the emitter surface. The SRV scales only with the electron concentration near the surface and thus is constant for the first 20 nm of emitter surface removal. It can be extracted from J_{0e} values for samples with removed supersaturated region.
- Case 2: The minority carrier lifetime in the supersaturated region is limited by Auger recombination, $\tau_{sat} = \tau_{Aug} = 133$ ps. The SRV scales with the phosphorus surface concentration $c_{Ph,surf}$ and is the only unknown parameter in the model. It can be extracted from the known J_{0e} values and concentration

profiles.

- Case 3: Similar to case 1, the SRV scales with the electron concentration near the surface. In contrast the minority carrier lifetime in the supersaturated region τ_{sat} is influenced by additional recombination. In a first crude assumption (3a) τ_{sat} is assumed to be constant. In a second approximation (3b) the additional recombination rate is assumed to be proportional to the local density of undissolved phosphorus (c_{Ph} - $c_{Ph,sol}$) giving

$$\tau_{sat} = [1/\tau_{Aug} + A \cdot (c_{Ph} - c_{Ph,sol})]^{-1}. \quad (1)$$

For case 2 the extracted SRVs represent an upper limit and show a power law dependence on the chemical phosphorus surface concentration $c_{Ph,surf}$ (Fig 3). We take the empirical fit-function from Ref [8], neglecting the first term since we only evaluate data for concentrations exceeding $4 \cdot 10^{19}$ cm^{-3}, yielding

$$S(c_{Ph,surf}) = S_p \cdot (c_{Ph,surf} / 10^{19}\text{cm}^{-3})^{\gamma}. \quad (2)$$

Table 2 shows the applied parameters. For cases 1 and 3 we consider only the extracted SRVs of not supersaturated samples. For $c_{Ph,surf} > n_{active}$ a constant value of $1.6 \cdot 10^5$ cm/s is used (see Fig 3).

Table 2. SRV of SiN_x-passivated planar phosphorus-doped surfaces, parameters for Eq. (2)

Parameter	Case 2	Cases 1 and 3 only for ($c_{Ph,surf} < n_{active}$)
S_p (cm/s)	$(47 \pm 12) \cdot 10^2$	$(30 \pm 1) \cdot 10^2$
γ	0.99 ± 0.06	1.26 ± 0.02

Our results deviate from published data for SiN_x-passivation [8] (not fired); however, this may partly originate from the applied firing step, allowing effective hydrogen passivation of the interface, and from the difference in stoichiometric composition of the different silicon nitride films. The obtained SRVs represent effective values, including a possible effect of surface charge, which is not considered in this work, but assumed to be negligible [8]. The power law fit (case 2) for concentrations exceeding the

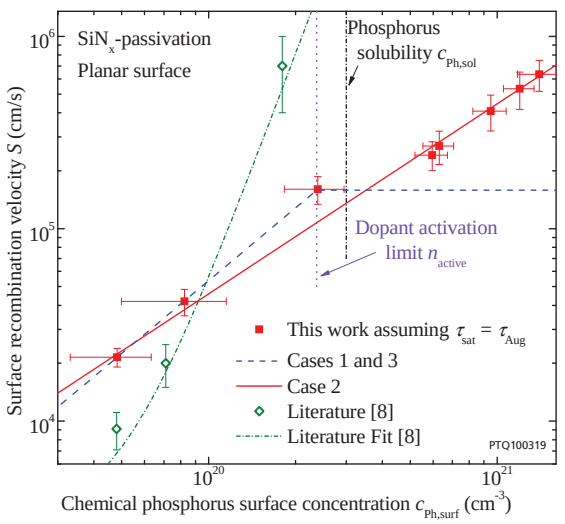

Fig 3. SRV vs. phosphorus surface concentration for SiN_x-passivated planar surfaces. The data points are extracted from measured J_{0e} assuming only Auger recombination in the emitter bulk. For cases 1 and 3, the parameterisation of the SRV considers only data of emitters without electrically inactive phosphorus. For comparison literature data is shown [8].

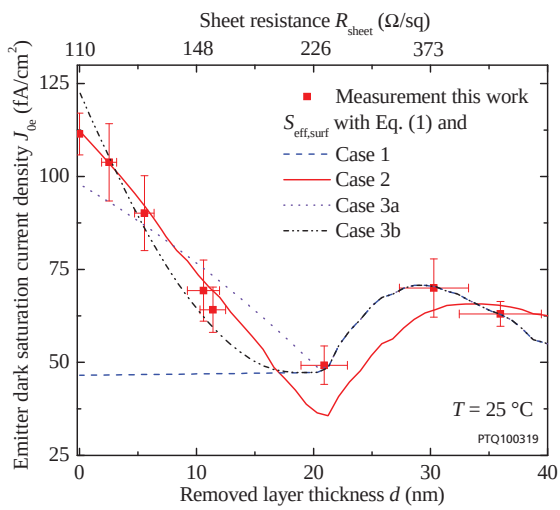

Fig 4. Measured (symbols) and simulated (lines) J_{0e} with SRV-fit from Fig 2, Eq. (2) for the four considered cases.

dopant activation limit [10] suggests that, assuming only Auger recombination in the emitter bulk, the SRV rather depends on the chemical phosphorus concentration than on the electron concentration.

2.3. Discussion

The fitted power law from Eq. (2) allows for the recalculation of J_{0e} as a function of the removed layer thickness (Fig 4).

- Cases 1 and 2: Assuming Auger-limited lifetime in the emitter bulk even for samples with high surface concentration and undissolved phosphorus the extracted SRVs suggest that the SRV depends on the chemical phosphorus surface concentration (case 2) rather than on the dissolved dopant or even electron concentration (case 1), which is an important distinction. The obtained SRVs have to be considered as an upper limit, since only Auger, radiative and constant low SRH recombination are included in the model.
- Case 3: Assuming that the SRV scales only with electron concentration, a strong reduction of the carrier lifetime in the supersaturated region τ_{sat} is needed to reproduce the experimental data. In this case, the assumption of an additional recombination rate proportional to the local concentration of undissolved phosphorus (case 3b) yields a slightly better agreement to the measured J_{0e} data than a constant reduced lifetime τ_{sat} in the supersaturated region (case 3a). The least squares fit give a proportionality factor $A = 5.5 \cdot 10^{-10}$ cm^3/s that lead to minority carrier lifetimes of 1.6 ps near the emitter surface in case 3b as well as a lifetime $\tau_{sat} = 7.5$ ps (case 3a) which is far below the predicted Auger lifetime of 133 ps.

After removing the supersaturated region ($d > 21$ nm) both parameterisations of the SRV together with the assumption of Auger-limited carrier lifetime provide the same behaviour as the measured J_{0e} values: the saturation current J_{0e} increases until it reaches a maximum at about $d = 30$ nm reflecting a maximum in the surface recombination current $J_{rec,surf} = q\, p_0\, S$ (see Fig. 3 and 5) as predicted by F-D-statistics. For $21 < d < 30$ nm ($2 \cdot 10^{20} > c_{Ph,surf} > 7 \cdot 10^{19}$ cm^{-3}) p_0 increases stronger than the power law for S decreases, whereas for $d > 30$ nm the decrease in S dominates $J_{rec,surf}$. It is worth mentioning that this qualitative behaviour could not be reproduced by the use of Boltzmann statistics and effective values, applying the same simple power law function (Eq. 2) for the SRV.

3. Conclusion

We present an analytical approximation for modelling highly phosphorus-doped emitters that shows very good agreement with numerical solvers. The analytical approach together with the simple power law fit for the SRV well describes the dependence of J_{0e} on the etched layer thickness for an etch-variation of 0 to 36 nm removal of emitter surface using F-D-statistics. Assuming only Auger-recombination in the supersaturated region, the extracted power-law dependence of the SRV on the chemical phosphorus surface concentration can be considered as an upper limit. Assuming a bulk recombination rate proportional to the concentration of undissolved phosphorus and a dependency of the SRV only on the electron surface concentration instead of the phosphorus concentration also shows good agreement with the given experimental data. Our results thus do not allow distinguishing between these two cases, but strongly support the assumption that either the SRV or the minority carrier lifetime in the supersaturated region or both are affected by the concentration of undissolved or electrically inactive phosphorus.

Acknowledgements

We gratefully acknowledge the technical support by the PV-TEC co-workers. This work is supported by the German Federal Ministry of Environment, Nature Conservation and Nuclear Safety under contract 0329849B.

References

[1] McIntosh KR and Altermatt PP. *A freeware 1d emitter model for silicon solar cells.* Proceedings of the 35th IEEE Photovoltaic Specialists Conference. Honolulu, Hawaii, USA, 2010. pp. 2188-2193.
[2] Cuevas A, Merchán R and Ramos JC. *On the systematic analytical solutions for minority-carrier transport in nonuniform doped semiconductors: Application to solar cells.* IEEE Transactions on Electron Devices, 1993; 40 (6): 1181-3.
[3] Klaassen DBM. *A unified mobility model for device simulation. I. Model equations and concentration dependence.* Solid-State Electronics, 1992; 35 (7): 953-9.
[4] Klaassen DBM. *A unified mobility model for device simulation--ii. Temperature dependence of carrier mobility and lifetime.* Solid-State Electronics, 1992; 35 (7): 961-7.
[5] Kerr MJ and Cuevas A. *General parameterization of auger recombination in crystalline silicon.* Journal of Applied Physics, 2002; 91 (4): 2473-80.
[6] Schenk A. *Finite-temperature full random-phase approximation model of band gap narrowing for silicon device simulation.* Journal of Applied Physics, 1998; 84 (7): 3684-95.
[7] Altermatt PP, Schenk A and Geelhaar F. *Reassessment of the intrinsic carrier density in crystalline silicon in view of band-gap narrowing.* Journal of Applied Physics, 2003; 93 (3): 1598-604.
[8] Altermatt PP, Schumacher JO and Cuevas A. *Numerical modeling of highly doped si:P emitters based on fermi-dirac statistics and self-consistent material parameters.* Journal of Applied Physics, 2002; 92 (6): 3187-97.
[9] Reichel C, Granek F, Benick J, Schultz Wittmann O and Glunz SW. *Comparison of emitter saturation current densities determined by injection dependent lifetime spectroscopy in high and low injection regimes.* Progress in Photovoltaics: Research and Applications, 2010
[10] Solmi S, Parisini A and Angelucci R. *Dopant and carrier concentration in si in equilibrium with monoclinic sip precipitates.* Physical Review B, 1996; 53 (12): 7836-41.
[11] Horzel J, Schum B and Lachowicz A. *On anomalous emitter regions forming during phosphorus diffusion processing of crystalline silicon solar cells.* Proceedings of the 25th European Photovoltaic Solar Energy Conference and Exhibition. Valencia, Spain, 2010. pp. 1882 - 1891.
[12] Wolf A, Biro D, Nekarda J-F, Stumpp S, Kimmerle A, Mack S et al. *Comprehensive analytical model for locally contacted rear surface passivated solar cells.* Journal of Applied Physics, 2010; 108 (124510): 1-13.
[13] Green MA. *Intrinsic concentration, effective densities of states, and effective mass in silicon.* Journal of Applied Physics, 1990; 67 (6): 2944-54.

Appendix A. Fermi-Dirac statistics

Modelling n-type emitter recombination strongly depends on the minority carrier density p_0, which is calculated in equilibrium from the intrinsic carrier density n_i with $n_i^2 = n_0 p_0$. The intrinsic carrier concentration in the emitter is influenced by BGN and must be calculated applying Fermi-Dirac statistics [8]. We use a simple FD-statistics correction, taking care to converge with experimental values of n_i for lower doped silicon (Fig 5). For undoped silicon, yielding $n_{i,0} = 9.65 \cdot 10^9$ cm^{-3} at $T = 300$ K [7], we use a temperature-parameterisation of $n_{i,0}$ as proposed in Ref. [12]

$$n_{i,0}(T) = 1.589 \cdot 10^9 \text{ cm}^{-3} \, (T / 1\text{K})^{1.706} \exp(-E_{g,0}(T)/2k_B T) \quad (3)$$

In this work, we apply a temperature-dependent band gap of undoped silicon $E_{g,0}(T)$ as well as the density of states $N_C = 2.86 \cdot 10^{19} \, (T / 300\text{K})^{1.58}$ cm^{-3} in the conduction band by Green et al. [13], Eq. (14) and (16). Including BGN and FD-statistics, this leads to the position of the electron Quasi-Fermi level E_{fn} in respect to the edge of the conduction band for undoped silicon $E_{C,0}$

$$E_{C,0} - E_{fn} = \Delta E_C - k_B T \, F_{1/2}^{-1}(n/N_C) \tag{5}$$

and the intrinsic carrier density [8]

$$n_i^2 = n_{i,0}^2 \, F_{1/2}([E_{fn} - E_{C,0} + \Delta E_C]/k_B T) \,/\, \exp(-[E_{C,0} - E_{fn}]/k_B T) \cdot \exp(\Delta E_V/k_B T)$$

$$= n_{i,0}^2 \cdot n/N_C \cdot \exp([E_{C,0} - E_{fn}]/k_B T) \cdot \exp(\Delta E_V/k_B T) \tag{6}$$

with ΔE_C and ΔE_V being absolute values from the full random phase BGN model of Schenk [6]. To evaluate the inverse Fermi integral $F_{1/2}^{-1}$ from Eq. (5), any analytical approximation as well as numerical solvers may be used.

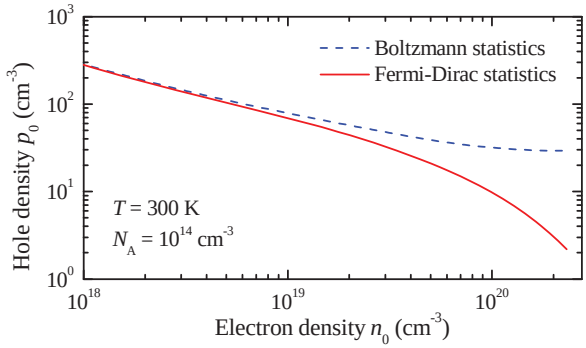

Fig 5. Hole density vs. electron concentration of highly n-doped silicon at thermal equilibrium calculated with Boltzmann and Fermi-Dirac statistics. The FD statistics converges with Boltzmann values for lowly doped silicon by construction. Boltzmann statistics overestimates the hole density significantly in highly doped silicon.